AAPM REPORT NO. 111

Comprehensive Methodology for the Evaluation of Radiation Dose in X-Ray Computed Tomography

A New Measurement Paradigm Based on a Unified Theory for Axial, Helical, Fan-Beam, and Cone-Beam Scanning With or Without Longitudinal Translation of the Patient Table

Report of AAPM Task Group 111:
The Future of CT Dosimetry

February 2010

ISBN: 978-1-888340-94-5
ISSN: 0271-7344

Published by
American Association of Physicists in Medicine
One Physics Ellipse
College Park, MD 20740-3846

Report of AAPM Task Group III: The Future of CT Dosimetry

Task Group Members

Robert L. Dixon, Chairman
Dept. of Radiology, Wake Forest University School of Medicine
Jon A. Anderson
Dept. of Radiology, UT Southwestern Medical Center at Dallas
Donovan M. Bakalyar
Dept. of Radiology, Henry Ford Hospital
Kirsten Boedeker
Toshiba Medical Systems
John M. Boone
Dept. of Radiology, University of California Davis
Dianna D. Cody
The University of Texas M.D. Anderson Cancer Center
Rebecca Fahrig
Dept. of Radiology, Stanford University
David A. Jaffray
Princess Margaret Hospital, Toronto
Iacovos S. Kyprianou
U.S. Food and Drug Administration
Cynthia H. McCollough
Dept. of Radiation, Mayo Clinic Rochester
Michael F. McNitt-Gray
Dept. of Radiology, University of California Los Angeles
Hugh T. Morgan
Philips Healthcare
Richard L. Morin
Dept. of Radiology, Mayo Clinic Florida
Keith D. Nakonechny
CancerCare Manitoba
Thomas J. Payne
Abbott Northwestern Hospital
Robert J. Pizzutiello
Upstate Medical Physics

Task Group Members (continued)

Bernhard T. Schmidt
Siemens AG
Anthony J. Seibert
Dept. of Radiology, UC Davis Medical Center
William E. Simon
Sun Nuclear Corp.
Thomas W. Slowey
K&S Associates, Inc.
Stanley H. Stern
U.S. Food and Drug Administration
Paul Sunde
Radcal Inc.
Thomas L. Toth
GE Healthcare
Stephen Vastagh
MITA

Contents

1. INTRODUCTION

The current paradigm for characterizing radiation dose in computed tomography (CT) is based on a metric—the computed tomography dose index (*CTDI*)—introduced nearly thirty years ago[1] and subsequently adapted, for example, as $CTDI_{FDA}$, $CTDI_{100}$, $CTDI_{w}$, $CTDI_{vol}$, and dose-length product (*DLP*) to facilitate government regulation,[2] application at clinical facilities,[3,4] and manufacturer-consensus standardization of CT dosimetry.[5–7] Typically *CTDI* is applied to represent absorbed dose along an axis of a cylindrical phantom. Essentially *CTDI*

- corresponds to the average value of the multiple-scan dose profile over the central range $(-nT/2, nT/2)$ spanning the total width nT of a group of n (≥ 1) simultaneously acquired tomographic sections, each section of width T;
- is associated with the midpoint $(z = 0)$ of a scanning length L along the scanner longitudinal axis range $(-L/2, L/2)$ through which the phantom is stepped in a sequence of multiple, discrete, contiguously spaced exposures; and
- is acquired with each exposure made in an axial-scanning mode, i.e., where there is no table movement during irradiation while the x-ray source rotates around the system isocenter.

Because formally, mathematically, this multiple-scan average is equivalent to the single-rotation dose profile (per total beam width) integrated over $(-L/2, L/2)$, it is convenient to assess the magnitude of *CTDI* during a single rotation: typically its value is approximated via measurement with a fixed-length—usually 100 mm—relatively long "pencil" ionization chamber symmetrically straddling the fan-beam plane. With this configuration $CTDI_{100}$ designates a reference index of dose accumulating at $z = 0$. For this index, the ionization chamber length, fixed at 100 mm, represents a standardized scanning length $L = 100$ mm over which the phantom dose profile is integrated, by convention irrespective of any particular scanning length actually used in a clinical examination of an individual patient. $CTDI_{100}$ measurements are usually carried out with the ionization chamber placed in a cylindrical, polymethyl methacrylate (PMMA) dosimetry phantom and aligned along the phantom's central axis ($CTDI_{100,c}$)—along the axis of rotation—or along one of the phantom's peripheral axes ($CTDI_{100,p}$).[1] In the current CT dosimetry paradigm, PMMA phantoms are typically 14- to 15-cm long and of 16-cm or 32-cm diameter, where the latter two dimensions are intended to correspond in a gross sense to the breadth of an adult head or adult torso, respectively.[2] It is also possible to measure *CTDI* free-in-air ($CTDI_{air}$), i.e., with no phantom present.

Since the introduction of *CTDI*, there have been revolutionary advances in CT technology,[8] in the application of these advances to the development of novel and improved clinical procedures,[9] and in the proliferation of CT utilization[10–12] involving new modes of operation,

[1] By convention for the $CTDI_{100}$-based family of indices, *air* is the reference medium to which absorbed dose values refer regardless of whether measurements are carried out free-in-air or within a PMMA dosimetry phantom serving as an absorption and scattering material.

[2] For pre-programmed protocols applied in pediatric exams done with some CT scanner models, the 16-cm diameter PMMA phantom may refer to a child's torso. This convention is not standardized across CT models of all manufacturers.

e.g., helical scanning and cone-beam irradiation geometries, for which *CTDI* as initially conceived was not defined. *CTDI* is defined exclusively for axial scanning, and its application to characterize dose in helical scanning is therefore conceptually presumptuous. Furthermore, trends toward wider and wider longitudinal (z)-axis collimations and toward longer scanning lengths tend to limit the accuracy, clinical relevance, and practical utility for $CTDI_{100}$-based parameters to represent CT dose: as $CTDI_{100}$ excludes contributions from radiation scattered beyond the relatively short (100-mm) range of integration along z, it tends to undervalue the cumulative dose at $z = 0$ that would otherwise be reported were all contributions included.[13–17] This underestimation is systematic, applying to narrow and wide beams alike, and slowly becomes larger with increasing width of the z-axis collimation.[15]

Even more problematic is the advent of cone-beam CT systems with beam widths along z sufficiently broad to image the anatomy of interest in a single rotation (or in multiple rotations) without table movement. Conceptually, *CTDI* is not an appropriate index for a stationary phantom because its integral form is the direct result of table/phantom translation over the range L, and its divisor nT is actually just the particular value of the translation interval for contiguous scanning. Furthermore, some cone beams are broader than 100 mm, and as a practical matter, a 100-mm pencil ionization chamber is insufficiently long to register all of the primary radiation, let alone all of the scatter radiation. The limitations of *CTDI*, particularly $CTDI_{100}$, have been a compelling motivation for developing metrics robust enough to represent generic patient-relevant radiation doses accurately, irrespective of the CT scanner mode of operation now and into the foreseeable future.

This report summarizes theoretical, computational, and experimental results[18–27] that are the underpinning of these proposed new metrics and consolidates them in a new system for CT dosimetry applicable to the acceptance testing and quality control of CT equipment.[3] Moving beyond the limitations of $CTDI_{100}$, this system (1) uses a common measurement method and set of equations directly applicable to helical and axial modes of scanning employing table translation and is also applicable to fan- and cone-beam modes of operation without table translation, (2) is valid for any beam width, table increment, and scanning length, and (3) is suitable for any phantom shape—not limited to right-circular cylinders—of an appropriately long phantom having a uniform cross section and uniform composition along z. The intent is to make available an accurate approach for specifying CT radiation doses based on a theoretically coherent measurement methodology that can be readily implemented by medical physicists and that can be supported by manufacturers, standards developers, and regulators.

2. THEORETICAL, COMPUTATIONAL, AND EXPERIMENTAL UNDERPINNINGS

2.A. CUMULATIVE DOSE FOR FAN-BEAM AXIAL- OR HELICAL-MODE SCANNING WITH TABLE/PHANTOM TRANSLATION

The cumulative dose resulting from scanning a phantom moving along the z-axis (i.e., longitudinally) through a rotating x-ray fan beam or cone beam can be conceptualized as a buildup of

[3] See section 4 for a glossary of the symbols and terminology used in this report.

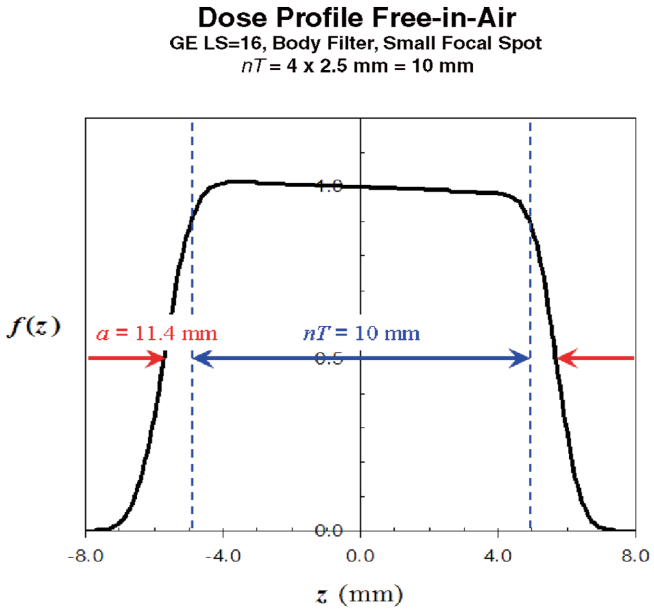

Figure 1. Dose profile $f(z)$ free-in-air modeled for a General Electric LightSpeed-16 scanner with a collimation width of $a = 11.4$ mm.[23] a corresponds to the full-width at half-$f(0)$ of the primary beam dose profile, and it is associated with a total nominal width $nT = 10$ mm of four adjacent 2.5-mm wide tomographic sections simultaneously acquired in a single scan.[23] Also evident is the heel effect.

dose resulting from the superposition of stationary, longitudinally displaced single-scan[4] dose profiles.[1] A scan is associated with a z-axis collimation width[5] a sufficiently broad to preclude penumbral interference with data acquisition in imaging a group of tomographic sections of total width[6] nT. Fig. 1 depicts the dose profile free-in-air for a single scan done with no table translation, and it illustrates the difference in values between a and nT. Parameter a represents a geometric projection onto the axis of rotation of the width of the physical opening of the pre-patient, z-axis collimator. The total width nT of the simultaneously acquired tomographic sections, on the other hand, represents an image parameter, viz., the nominal value of the overall width

[4] An individual scan generally refers to a process of x-ray tube rotation, irradiation, and data acquisition producing either one image associated with one ($n = 1$) tomographic section (single "slice" CT) or, in multiple-detector-row CT (MDCT), a group of images respectively associated with multiple ($n > 1$), adjacent tomographic sections simultaneously acquired during the single scan.

[5] Parameter a is the width along the axis of rotation of the pre-patient z-axis collimator geometrically projected from the centroid of the x-ray source. Parameter a corresponds to the full-width-at-half-$f_p(0)$ of the primary-beam dose profile $f_p(z)$.[27] In the text, "collimation width" is used interchangeably with "a" and refers to a geometric projection of the pre-patient z-axis collimator width onto the axis of rotation.

[6] nT is denoted $N \times T$ in international standards.[5–7] nT is commonly approximated by the total nominal width (projected to the axis of rotation) of the contiguous rows (or groups of contiguous rows) of detectors directly contributing to image formation in MDCT. For example, with an MDCT system operating with 16 longitudinal rows of 1.25-mm wide imaging detectors, $nT = 16 \times 1.25$ mm $= 20$ mm. For detector-row signals added in groups of four, $nT = 4 \times 5.0$ mm $= 20$ mm. When image acquisition and reconstruction involve longitudinal overlap of simultaneously acquired tomographic sections, as they do when CT systems operate in a mode employing a "flying focal spot," then the value of nT needs to be adjusted to account for such overlap in order to properly evaluate the total nominal width of reconstructed sections.

(along z) of the volume imaged in a scan. There is a complex relationship between nT and a, and their values are not generally the same.[23]

In axial scanning with table/phantom translation, one models a series of N identical rotations comprising a sequence of scans. The midpoint-to-midpoint spacing between successive scans is a constant interval b, and the range along the z-axis over which scanning is done is denoted by length $L = Nb$. This modeling of axial scanning represents a quasi-periodic, oscillatory dose distribution of fundamental period b.[18] [7] Smoothing the distribution by taking the "running mean," i.e., averaging over an interval $z \pm b/2$ at each value of z, yields an expression for the cumulative dose $D_L(z)$ as a convolution:[18]

$$D_L(z) = \frac{1}{b} f(z) \otimes \Pi(z/L) = \frac{1}{b} \int_{-L/2}^{L/2} f(z - z')\, dz'. \tag{1}$$

Along a particular longitudinal axis parallel to the axis of rotation, e.g., the central axis or a peripheral axis, $f(z)$ is the associated dose profile resulting from a single axial rotation centered about $z = 0$ in a stationary phantom. It includes both the primary-beam (p) and scatter-radiation (s) contributions, i.e., $f(z) = f_p(z) + f_s(z)$, and therefore $f(z)$ in a phantom is much broader than the full-width at half-$f(0)$ of the primary-beam dose profile $f_p(z)$.[29] $\Pi(z/L)$ is the rectangular function of unit height and length L, where L is the distance through which the full dose profile $f(z)$ is translated during a sequence of scanning. Fig. 2 depicts a group of cumulative dose profiles $D_L(z)$ resulting from scanning over various L.

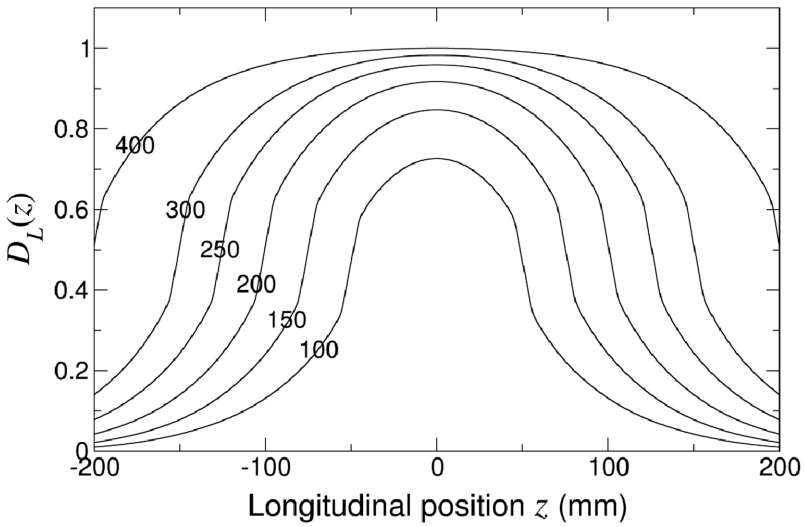

Figure 2. Cumulative dose distributions $D_L(z)$ for various scanning lengths L from 100 mm to 400 mm along the central z-axis of an elliptical cross-section water-equivalent phantom (Computerized Imaging Reference System, Inc.) with minor and major axes of 20 cm and 30 cm. $D_L(z)$ values are normalized to equilibrium dose (see text) $D_{eq} = 1$, and they are generated from the convolution Eq. (1) using the measured dose profile $f(z)$.[20]

[7] For examples illustrating such quasi-periodicity, see Ref. 1, Figs. 3–5 and Ref. 28, Fig. 2.

Evaluation of Eq. (1) at $z = 0$ provides the cumulative dose at the midpoint of the scanning range,

$$D_L\left(z=0\right)=\frac{1}{b}\int_{-L/2}^{L/2} f\left(z'\right)dz', \tag{2}$$

which represents an average over a typically small interval $(-b/2, b/2)$ about $z = 0$, where the scan interval b is typically much shorter than the total scanning length L, i.e., $b << L$. Note that since $L = Nb$, the limits of integration are implicitly related to the divisor b.

As the scanning length L increases, the cumulative dose at $z = 0$, i.e., the "central" cumulative dose," increases with accumulating contributions from the "scatter tails" of outlying scan sections. $D_L(z = 0)$ increases asymptotically toward an upper limiting value such that the source of scatter radiation is sufficiently remote so as to make negligibly small additional contributions. This limiting value is called the "equilibrium dose" D_{eq} and is given by

$$D_{eq}=\frac{1}{b}\int_{-\infty}^{\infty} f\left(z'\right)dz' \propto a/b. \tag{3}$$

The right-hand term indicates the functional dependence of $D_{eq} = D_{eq}(a,b)$ on collimation width a, to which the primary beam fluence incident on the phantom is directly proportional,[23] and on scan interval b, a decrease in which results in increasing overlap of individual dose profiles and thus an increase in the cumulative dose.[18]

As L increases, the central cumulative dose $D_L(z = 0)$ tends to approach the equilibrium value D_{eq} first, i.e., before any other value $D_L(z \neq 0)$ of cumulative dose would (cf. Fig. 2). To distinguish the asymptotic behavior of the central cumulative dose from that of $D_L(z \neq 0)$, and for purposes of dose evaluation precluding measurements over infinitely long ranges, it is convenient to introduce a parameter L_{eq} called the "equilibrium scanning length." L_{eq} is defined as a *finite* scanning length for which $D_{Leq}(z = 0)$ may be deemed to be close enough to the value D_{eq} to represent it practically; section 2.A.2 of this report describes the convention adopted for evaluating L_{eq}. For the particular phantom represented in Fig. 2, $L_{eq} \approx 400$ mm (and $L_{eq} \approx 450$ mm for the 32-cm diameter right-circular cylinder PMMA body phantom). As L increases further ($L > L_{eq}$), the region over which scatter equilibrium exists expands beyond $z = 0$, producing a flat central region about $z = 0$. The dose $D_L(z = \pm L/2)$ at the endpoints of a scanning length approaches ½ D_{eq} as the scanning length $L > L_{eq}$ approaches the full-width at half-maximum of the distribution $D_L(z)$. The *average* dose over $(-L/2, L/2)$ is less than the central cumulative dose $D_L(z = 0)$ for any value of L and approaches $D_L(z = 0) \approx D_{eq}$ only for scanning lengths $L >> L_{eq}$. To a good approximation[23] the dependence of D_{eq} on a/b (Eq. 3) applies likewise to the cumulative doses expressed in Eqs. (1) and (2) even for sub-equilibrium scanning lengths $L < L_{eq}$, where the dependence on a is approximate and on $1/b$ exact.[23,27]

In helical scanning, the scanning length L corresponds to the range along the longitudinal axis through which the table travels continuously during a sequence of scans.[8] $L = vt$, where v is the constant velocity of the patient table during x-ray tube rotation, irradiation, and data acquisition. t is the total time of x-ray tube loading, i.e., the total "beam-on" time (also referred to as tube "loading time" in the international standard[7]). Eqs. (1)–(3) apply to helical as well as to axial scanning, and they give the actual absolute dose on the phantom central axis. This dose is naturally smooth (non-oscillatory) for helical scanning in a cylindrical phantom, and no averaging is necessary.[18] On the peripheral axes, the helical-scanning dose is quasi-periodic along z with a period $b = v\tau$ equal to the table advance per rotation, where τ is the period of rotation. Eqs. (1)–(3) likewise apply to the helical dose on the peripheral axes if an angular average over 2π at a fixed z is used to smooth the distribution rather than the longitudinal running mean (as used for axial scanning).[18] Such smoothing allows the application of Eqs. (1)–(3) to both helical and axial scanning modes; and, where equilibrium exists, the respective helical and axial average cumulative doses converge to the same value for the same value of b.[23] [9]

D_{eq} is the basis of a robust dose metric applicable to the most frequently used scanning modes, is applicable to the evaluation of total energy absorbed (integral dose) in a phantom irrespective of scanning length, and is representative of the magnitude of cumulative dose that would be delivered clinically for scanning lengths $\sim L_{eq}$.[15,18–23] For clinical scanning lengths that are shorter than L_{eq}, section 2.A.2 describes an empirical relationship between the central cumulative dose and D_{eq}. Hence D_{eq} and its related parameters comprise a concise characterization of CT-scanner dose, and the description of their measurement is the principal goal of this report.

2.A.1. Cumulative dose parameterization, scan contiguity, and geometric efficiency

For convenience of measurement and dose estimation, we develop two alternative parameterizations of dose quantities, the first independent of b and the second independent of a as well as b. As a preliminary step, we define a "generalized pitch" factor, i.e., one applicable for either axial or helical scanning,

$$p = \frac{b}{nT}, \tag{4}$$

which quantifies the longitudinal overlap ($p < 1$), gap ($p > 1$), or contiguity ($p = 1$) between successive groups of tomographic sections. In Eq. (4) parameter b is generalized in the sense that it corresponds either to the table increment (scan interval) in a sequence of axial scanning or to the continuous table advance per rotation ($b = v\tau$) during helical scanning.[23,27] For n reconstructed

[8] In helical scanning, the scanning length L for irradiation can automatically exceed the image-reconstruction range of clinical interest that an operator would select on the basis of pre-scanning scout preview images. Such "over-ranging" by the system ensures that the tomographic reconstruction algorithms have sufficient information beyond the selected range of clinical interest so as to render accurate interpolations within the clinical range.

[9] The rotational irradiation geometry of a CT scanner has no bearing on the applicability of this theory, which will work just as well for a non-rotational fan-beam acquisition ("scout view" or scan projection radiography), and the preceding equations can be readily adapted to such a case.

tomographic sections, each of nominal width T, nT is the total nominal width (along the axis of rotation) associated with the group of sections simultaneously acquired and yielding multiple images associated with a single scan.

Since the equilibrium dose $D_{eq} = D_{eq}(a,b)$ is proportional to the ratio a/b and by definition is acquired at pitch $p = \frac{b}{nT}$, $D_{eq}(a,b) = D_{eq}(a,p) \propto \frac{1}{p}\frac{a}{nT}$. Hence the first alternative parameterization is the *equilibrium dose-pitch product*

$$\hat{D}_{eq} \equiv p \cdot D_{eq}(a,p) \propto \frac{a}{nT}, \tag{5}$$

which is independent of p (or b) and is identical to the equilibrium dose $D_{eq}(a,p)$ for a generalized pitch p of unity.[10] For example, for two separate sequences of scanning, one with pitch p_1 and the other with pitch p_2, if each sequence is done with the same collimation width a and total section width nT, then $p_1 \cdot D_{eq}(a,p_1) = p_2 \cdot D_{eq}(a,p_2) = \hat{D}_{eq}(a)$, independent of pitch (or scan interval b). The same principle applies to the product of the cumulative (non-equilibrium) dose $D_L(z = 0)$ and pitch: $\hat{D}_L \equiv p \cdot D_L(z = 0; a, p)$ is independent of p (or b). The pitch independence of $\hat{D}_{eq}$ and of $\hat{D}_L$ allows one to choose a practical value of the acquisition pitch for the purpose of acceptance-test and quality-control measurements irrespective of any pitch p_c used clinically, which may not be suitable for measurement, and subsequently infer a dose D_c at the clinical technique from the relation $D_c = \hat{D}/p_c$ (where, according to the particular situation, $\hat{D}$ may represent either the equilibrium $\hat{D}_{eq}$ or a non-equilibrium $\hat{D}_L$ dose-pitch product).

The second alternative parameterization we introduce is the *equilibrium dose constant*, defined as the following product:

$$(b/a) \cdot D_{eq} = (b/a) \cdot D_{eq}(a,b) = (nT/a) \cdot pD_{eq}(a,p) = (nT/a) \cdot \hat{D}_{eq}, \tag{6}$$

which, as indicated in Eqs. (3) and (5), is independent of a as well as b (and independent of pnT).[11] The *equilibrium dose constant* physically represents the equilibrium dose that would result were the table increment b to equal the collimation width a (or were pitch $p = a/nT$). On a given phantom axis for a particular set of operating conditions, a single evaluation of the equilibrium dose constant $(b/a) \cdot D_{eq}$ is tantamount to a complete specification of the dose on that axis: that is, a measurement of the equilibrium dose $D_{eq}(a,p)$ at a single known value of the collimation width a suffices for the computation of $(b/a) \cdot D_{eq}$, from which the equilibrium dose D_{eq} or equilibrium dose-pitch product $\hat{D}_{eq}$ can be rigorously obtained by scaling the equilibrium dose constant to any other collimation width a: D_{eq} and $\hat{D}_{eq}$ are each directly proportional to a. In other words, evaluation of $(b/a) \cdot D_{eq}$ is an accurate and robust shortcut that can reduce the number of measurements needed to represent doses.

---

[10] $\hat{D}_{eq}$ is equal to *CTDI* as originally defined per Ref. 1, i.e., associated with an infinite range of integration.

[11] The independence of the product $(b/a) \cdot D_{eq}$ from a and b has been demonstrated experimentally[23,24,27] for fan-beam axial and helical scanning as well as for cone beams.[21,24]

However, the collimation width a is not as readily determined as nT. In MDCT, the practice (commonly referred to as "over-beaming") of keeping the primary beam penumbra beyond the location of detectors used to reconstruct images generally necessitates that $a > nT$, as illustrated in Fig. 1, where any particular value of the ratio $a/(nT)$ depends in a complex way on focal spot size, selected detector configuration, and reconstruction algorithm such that there is not necessarily a unique correspondence between a value of nT and a single value of a.[30] [12] The same value of nT can correspond to different combinations of n and T, e.g., nT = 10 mm = 16×0.625 mm, 8×1.25 mm, and 4×2.5 mm, and associated with each such combination may be a slightly different collimation width a.[23,27]

For systems without post-patient collimation, correspondences between values of nT and a may be inferred from the following approximation for the *geometric efficiency in the z-direction*, which represents the fraction of free-in-air dose actually utilized for image reconstruction:[7] [13]

$$\begin{aligned} nT/a &\approx \textit{geometric efficiency in the z-direction} \\ a/(nT) &\approx \textit{over-beaming factor}. \end{aligned} \tag{7}$$

Setting $a > nT$ ("over-beaming") keeps the penumbra of the x-ray field extended beyond the locus of active detector elements that are spread over width nT (where all width values are understood by convention to be geometrically projected to the axis of rotation).[1] The geometric efficiency, approximated by nT/a, is the fraction of the free-in-air radiation dose utilized in creating the images (with detector septa ignored); it is equal to 88% in the example represented in Fig. 1.

For some CT scanners operating under particular scanning conditions, and for others under all conditions, the value of the *geometric efficiency in the z-direction* may be displayed on the CT console as a percentage. For all CT systems in compliance with the third edition of the International Electrotechnical Commission standard IEC 60601-2-44, tables of geometric efficiencies for all beam collimations are provided to customers in the documents accompanying the scanners.[7] From these tables one can use Eq. (7) to estimate the typical collimation width a associated with every possible combination of n and T used clinically. Alternatively, for a particular value of the total nominal width of a group of tomographic sections, say $n_1T_1 \geq 10$ mm, a corresponding estimate of the collimation width a_1 can be obtained directly from the full-width at half-$f(0)$ of the exposure distribution (free-in-air on the axis of rotation) imaged with a ready-pack film or other device such as an optically stimulated luminescence (OSL) imager. Since the infinite integral (free-in-air on the axis of rotation) of the dose profile is proportional to a, the value a_j associated with any other combination of n_j and T_j can be inferred from the ratio of a_1 to this infinite integral (for n_1, T_1) times the value of the infinite integral measured for n_j and T_j. (Also see section 2.D of this report.)

[12] Adaptive collimation[31] is an example of a technology developed to reduce over-beaming.

[13] Neither the ratio in Eq. (7) nor the IEC definition[7] of *geometric efficiency in the z-direction* accounts for the spatial inefficiency introduced by the presence of electronically passivated septa, which do not directly contribute to image formation but are needed to separate active elements of detector rows.

The following observations[23,27] underscore the magnitude of difference between a and nT and the role these factors play with respect to the equilibrium dose-pitch product $\hat{D}_{eq}$ versus the equilibrium dose constant $(b/a) \cdot D_{eq}$:

- $\hat{D}_{eq}$ is directly proportional to the *over-beaming factor* $a/(nT)$, and it can therefore vary by nearly a factor of *two* over the range 2.5 mm < nT < 20 mm.
- $(b/a) \cdot D_{eq}$ remains constant over the same range, 2.5 mm < nT < 20 mm.
- Efficiency generally improves the larger the value of nT.
- While $(b/a) \cdot D_{eq}$ does remain constant with respect to z-axis collimation, it varies according to scanner model, kVp, and shaped filtration.

2.A.2. Central (z = 0) cumulative dose and its approach to equilibrium

An estimate of the equilibrium dose D_{eq} can be obtained through a study of how the dose $D_L(z = 0)$ at the midpoint of the scanning length changes with L. Also, it is informative, especially for clinical situations where the scanning length L may be relatively short compared to L_{eq}, to quantify the dependence of the central cumulative dose $D_L(z = 0)$ on L to indicate peak cumulative dose values that can be significantly less than D_{eq}.

$D_L(z = 0)$ may be characterized empirically as a product of a dimensionless "approach-to-equilibrium function" $h(L)$ and the equilibrium dose D_{eq}:[27]

$$D_L\left(z=0\right) = h\left(L\right) D_{eq}, \tag{8}$$

where $h(L) \to 1$ when L becomes large enough to yield scatter equilibrium at $z = 0$. As was demonstrated for a 32-cm diameter PMMA phantom for scanning lengths L greater than the collimation width a, $h(L)$ has an approximate form as a constant plus an exponentially dependent term leading to saturation,[27]

$$h\left(L\right) \approx \left(1-\alpha\right) + \alpha\left[1-\exp\left(-4L/L_{eq}\right)\right] = 1-\alpha\exp\left(-4L/L_{eq}\right). \tag{9}$$

Hence from Eqs. (8) and (9) the equilibrium dose D_{eq} and the "equilibrium" scanning length L_{eq} can be evaluated as two elements of a set of three fit parameters, $\{\alpha, L_{eq}, D_{eq}\}$, for which the specific values would in general depend on phantom radial dimensions as well as on scanner-specific irradiation conditions. The term $(1 - \alpha)D_{eq}$ corresponds to the contribution of the primary radiation to the cumulative dose D_L at $z = 0$, and the term $\alpha[1 - \exp(-4L/L_{eq})]D_{eq}$ corresponds to the scatter-radiation contribution at $z = 0$.[14] With this parameterization, we identify by convention L_{eq} with that particular length L for which $\exp(-4L/L_{eq}) = \exp(-4) \approx 0.0183$, i.e., for which the central ($z = 0$) cumulative dose is within 2% of the limiting equilibrium value D_{eq}. In other words, L_{eq} is a finite scanning length with respect to which scanning of a longer range makes for practical purposes a negligibly small difference in the estimation of D_{eq}.

[14] The constant α of Eq. (9) is related to the scatter-to-primary ratio (SPR) extant on the phantom axis,[23] and it increases with increasing SPR. α is only slightly less than unity on the central axis of large-diameter phantoms where scatter dominates the primary dose contribution.

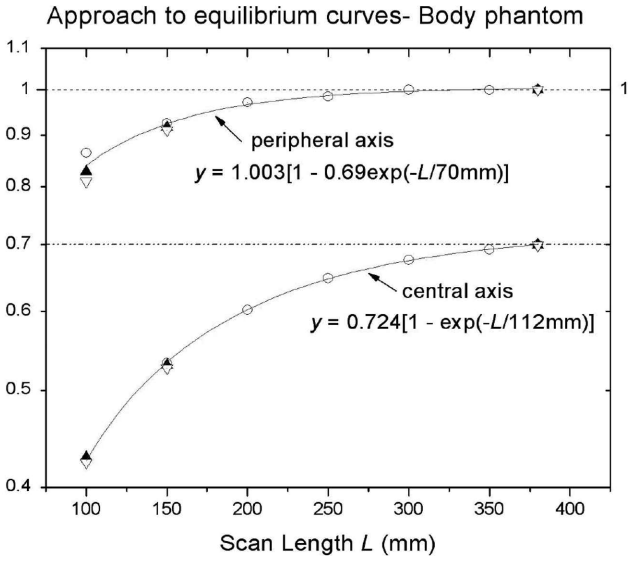

Figure 3. Approach to equilibrium of peripheral- and central-axis central cumulative doses $D_L(0)$ (both sets normalized to the peripheral-axis $D_{eq} = 1$) at 120 kVp.[27] Measured values: General Electric (GE) LightSpeed-16 with $nT = 20$ mm; ▲ GE VCT with $nT = 20$ mm; ∇ GE VCT with $nT = 40$ mm.

The data in Fig. 3 indicate that the formula for $h(L)$ is relatively more robust for central-axis doses, where scatter contributions dominate and α is close to unity, than for peripheral-axis doses, where at $L = 100$ mm the largest variation of measured values occurs. For routine field work on a particular scanner, Fig. 3 and Eqs. (8) and (9) also suggest the possibility of using shorter length, more manageable phantoms, for which previously estimated values of α and L_{eq} have been validated, to estimate D_{eq} through extrapolation. If α and L_{eq} are not known *a priori* however, then extrapolation would require dose measurements at several values of $L > a$, including a measurement at the largest value of L practicable.

Monte Carlo simulations[15] confirm that $h(L)$ has a relatively weak dependence on the z-axis beam collimation width a and thus on the nominal width nT of the tomographic sections imaged: the variation of $h(L = 100$ mm) with a is less than 1.5% over the range 1 mm $\leq a \leq 40$ mm for all kVp settings from 80–140 kVp for both the head and body PMMA phantoms. Moreover, these simulations show that $h(L = 100$ mm) varies by <5% over 80–140 kVp and by <2.5% over 100–140 kVp. The relatively weak dependencies of $h(L)$ on a and on kVp suggest that once $h(L)$ is evaluated, its application to other cases can be exploited to reduce the number of measurements needed to characterize dose for various CT conditions of operation.

2.B. CUMULATIVE DOSE FOR SINGLE- OR MULTIPLE-ROTATION FAN-BEAM OR CONE-BEAM SCANNING WITHOUT TABLE/PHANTOM TRANSLATION

For a phantom fixed on a non-translating table and undergoing a series of N rotations, the cumulative dose $D_N(z)$ is simply related to the dose profile $f(z)$ for a single axial rotation:

$$D_N(z) = Nf(z), \tag{10}$$

and hence the central cumulative dose at $z = 0$ is given by

$$D_N(0) = Nf(0). \tag{11}$$

Estimates of the peak value $f(0)$ could be especially useful to characterize the magnitude of dose in procedures involving CT fluoroscopy,[32,33] which involve fan beams and where a patient may be subject to skin injury from exposure involving multiple x-ray source rotations about a circumferential area of the skin that is relatively stationary with respect to the fan-beam plane. If the collimation width a is wider than the length of the thimble ionization chamber used for measurements (section 3.C), then $f(0)$ is readily determined as a "point dose" measurement with this small ionization chamber located on the central ray at $z = 0$. However, for collimation widths a that are narrower than the length of the small ionization chamber, it will be necessary to use an alternative, appropriately small dosimeter to evaluate $f(0)$, such as a small solid-state detector[20,21] or thermoluminescent dosimeter (TLD) properly corrected for photon energy response. Such point dosimeters may also be used to measure the entire axial dose profile $f(z)$.[20,21]

CT systems having beam widths along z wide enough to cover a significant anatomic range in a single rotation are rapidly proliferating in the clinic. Some of these systems utilize a conventional CT platform, can provide either helical or axial scanning modes involving table translation, and can also provide single- or multiple-rotation acquisitions with a stationary table (i.e., at a fixed z-location). Stationary-table scanning is used primarily in perfusion studies, and this technique may also be combined with CT angiography to produce cardiac images from rapid, sub-second scans, for example, with a 40-mm beam width in 64-detector-row systems, and also with selectable beam widths ranging from 40 mm up to 160 mm in one 320-detector-row system recently introduced.[34]

For a single rotation of a cone beam about a stationary phantom, the appropriate measurement to make would be that of the dose at the midpoint of the irradiated length; since the cone beam width a is typically much larger than the ionization chamber length, a direct measurement of the central ray dose $f(0)$ is the simplest and most straightforward measurement method for the dose delivered using these wide cone beams. Such a dose value would be analogous to that characterizing the dose in fan-beam axial or helical CT scanning with table/phantom motion. The physics suggests that one can conceptualize a wide primary cone beam of width a in a stationary phantom as a group of N adjacent, narrow primary beams each of width a/N, spaced at intervals $b = a/N$ in a manner analogous to an axial-scanning sequence of length $L = Nb = a$ and thus "directly irradiating" the same length of phantom as would the cone beam. Since the length of the phantom "directly irradiated" is the same, the dose distributions in-phantom would likewise be nearly the same in both cases, i.e., $f(z)$ for a single rotation of a cone beam about a stationary phantom would approximately equal $D_L(z)$ for fan-beam scanning—cf. Eqs. (1) and (2)—with $b = a/N$. Thus the dose at $z = 0$ would be described equally well by $f(0)$ for the cone beam or by $D_L(0)$ for an equivalent group of adjacent narrow beams covering the same length $L = a$. This analogy suggests a direct physical connection between the dose in axial or helical fan-beam CT with table translation and that in stationary-phantom cone-beam CT: since the dose on the central ray of the cone beam at $z = 0$ is the direct mathematical and physical analog of the central cumulative dose $D_L(0)$ in axial or helical CT, then $f(0)$ is

the obvious choice of the dose to measure and report for stationary-phantom cone-beam modes of scanning. The mathematical formalism automatically forces the same logical conclusion, i.e., as the table increment $b \to 0$ (no phantom motion), the dose $D_L(0)$ given by Eq. (2) smoothly approaches the value $Nf(0)$ given by Eq. (9) due to the fact that $L = Nb$, and the integration limits $\pm L/2$ likewise approach zero. Like $D_L(z)$, the cone-beam dose $f(0)$ would approach a maximum equilibrium value $f_{eq}(0)$ were the total cone beam width a increased to a value wide enough to achieve scatter equilibrium on the central ray at $z = 0$ such that further increases in a would not affect the dose at $z = 0$. However, evaluation of $f_{eq}(0)$ is generally not clinically relevant in the case of a stationary phantom, since cone beams of width $a_{eq} = L_{eq} > 400$ mm are not usually used in single-rotation acquisitions (except possibly by CT systems employing C-arm, flat-panel detectors).

2.C. INTEGRAL DOSE AND PLANAR AVERAGE EQUILIBRIUM DOSE

The integral dose E_{tot} (i.e., the total energy absorbed in the phantom) serves as a simplified indicator of patient risk: the presumption is that cancer risk increases the larger the dose and irradiation volume containing radiosensitive tissue. While more relevant to the concern about radiation risk than to acceptance testing and physics calibrations *per se*, E_{tot} and an associated derivative quantity, the planar average equilibrium dose $\bar{D}_{eq}$, may be informative to the CT operator, radiologist, and those concerned with assessing public health implications of radiation dose for various CT scanning techniques. $\bar{D}_{eq}$—or the closely related parameterizations $\hat{D}_{eq}$ and $(b/a)\cdot\bar{D}_{eq}$—could prove valuable as a basis for comparisons of values associated with different scanners and also possibly as a reference quantity to which organ dose estimates could be normalized so as to make such normalized estimates practically independent of scanner model.[35,36]

Denoting $f(r,z)$ as the single-rotation, axial dose profile along a given z axis located at radius r from the central axis, and integrating over both r and z, one can calculate the total energy absorbed in the entire volume of a phantom of mass density ρ. For N adjacent rotations each spaced at interval b with respect to one another, the energy deposited in a cylindrical phantom of radius R and mass density ρ is given by the product of N and the energy deposited per single rotation:

$$E_{tot} = N\rho\int_{-\infty}^{\infty}\int_{0}^{R} f(r,z)2\pi r dr dz = \rho Nb\int_{0}^{R} 2\pi r dr\left\{\frac{1}{b}\int_{-\infty}^{\infty} f(r,z)dz\right\} = \rho L\int_{0}^{R} D_{eq}(r)2\pi dr, \qquad (12)$$

where Eq. (3) for D_{eq} is used, and N is replaced by the spatial surrogate $L = Nb$.

Eq. (12) can be rewritten as

$$E_{tot} = \rho\pi R^2 L\left\{\frac{1}{\pi R^2}\int_{0}^{R} D_{eq}(r)2\pi r dr\right\} = \rho\pi R^2 L\bar{D}_{eq}, \qquad (13)$$

which is expressed in terms of the planar average (denoted $\bar{D}_{eq}$) of $D_{eq}(r)$ over the area πR^2 of the central scan plane, located at the midpoint $z = 0$ of the longitudinal scanning range of length L.

The following points elucidate important physics aspects of Eqs. (12) and (13):

- $E_{tot} = \rho\pi R^2 L\bar{D}_{eq}$ is *not* equal to the energy deposited inside the scanned volume $\pi R^2 L$, but rather it includes significant energy deposited beyond $(-L/2, L/2)$ by scattered radiation. Therefore division of E_{tot} by the directly irradiated mass $\rho\pi R^2 L$ does not equal the average dose over the scanned volume $\pi R^2 L$.
- Thus it follows that $\bar{D}_{eq}$ is *not* equal to the average dose over the scanned volume $\pi R^2 L$; moreover, there is no analytic expression for such an average dose.
- The relation $E_{tot} = \rho\pi R^2 L\bar{D}_{eq}$ is valid for any scanning length L, *even for sub-equilibrium scanning lengths*. So if, for a particular value of L, dose equilibrium has not been obtained, then to evaluate E_{tot} accurately, one must nevertheless use the equilibrium dose $\bar{D}_{eq}$ in Eq. (13).
- $N = t/\tau$ corresponds to the total x-ray beam-on time t, which is related to the *total mAs* on which E_{tot} fundamentally depends.
- For a given tube current and a given beam-on time t, i.e., for one particular *total mAs*, E_{tot} is independent of the scanning length L, where L depends on table velocity v. For example, say in case 1 the system is configured for 100 mAs per rotation, 1 rotation per second, $t_1 = 30$ s, and $v_1 = 10$ mm/s. Hence the total number of rotations = 30, and the *total* $mAs_1 = 30$ rotations $\times$ 100 mAs per rotation = 3000 mAs; and $L_1 = v_1 t_1 = 300$ mm. Now consider case 2: the system is configured just as in case 1 except for the table velocity: 100 mAs per rotation, 1 rotations per second, $t_2 = 30$ s and $v_2 = 5$ mm/s. In case 2, the total number of rotations = 30, the *total* $mAs_2 = 30$ rotations $\times$ 100 mAs per rotation = 3000 mAs; but $L_2 = v_2 t_2 = 150$ mm. Here's the point: because the *total mAs* is the same in both cases, the total integral dose E_{tot} is the same in both cases. The phantom would absorb the same amount of energy E_{tot} but in a smaller irradiation volume for case 2 than for case 1.

As the scanning length L increases, the cumulative dose radial distribution $D_L(z = 0; r)$ becomes relatively more uniform across r due to greater scatter buildup on the central phantom axis than on the peripheral axes, and thus the equilibrium dose $D_{eq}(r)$ exhibits a weaker radial variation than the cumulative dose $D_L(z = 0; r)$ for $L < L_{eq}$. Since dose measurements are typically made at only two values of r—on the phantom central ($r = 0$) and peripheral ($r = R - 10$ mm) axes—a "two-point" approximation to the radial integral in Eq. (13) can be made by assuming a plausible relative functional variation[37,38] of $D_{eq}(r)$ with r, e.g., $D_{eq}(r) \propto r^2$. Better approximations can be made determining a more exact functional form of $D_{eq}(r)$, which could be established by measurement or Monte Carlo simulation for the particular phantom and scanner being utilized.

Here is an example of the evaluation of the integral dose E_{tot} and its relation to the planar average equilibrium dose $\bar{D}_{eq}$: consider body scanning with a GE VCT 64-multiple-row detector CT (MDCT) system at 120 kVp, 250 mAs per rotation, with 10 contiguous 0.5-s rotations and $nT = 40$ mm. Under these operating conditions, $L \approx 10$ rotations $\times$ 40 mm per rotation = 400 mm = 40 cm = 0.400 m. The central and peripheral equilibrium doses in a

0.400-m long, 0.320-m diameter PMMA phantom were measured to be, respectively, $D_{eq,c}$ = 21.8 mGy and $D_{eq,p}$ = 32.4 mGy.[27] With the assumption that $D_{eq}(r) \propto r^2$, $\bar{D}_{eq}$ = ½ $D_{eq,c}$ + ½ $D_{eq,p}$ = 27.1 mGy. Applying Eq. (13) with ρ = 1190 kg/m^3, π = 3.14, R = 0.160 m, L = 0.400 m, and $\bar{D}_{eq}$ = 27.1 mGy = 0.0271 Gy = 0.0271 J/kg, where the units have been converted to kilograms, meters, and joules for convenience of calculation, one obtains

$$\begin{aligned} E_{tot} &= \rho\pi R^2 L \bar{D}_{eq} \\ &= 1190\ \text{kg/m}^3 \times 3.14 \times \left(0.160\ \text{m}^2\right) \times 0.400\ \text{m} \times 0.0271\ \text{J/kg} \\ &\approx 1\ \text{J}, \end{aligned}$$

independent of both pitch and scanning length, deposited in the phantom at a rate of (1 J)/(10 rotations × 0.5 s/rotation) = (1 J)/(5 s) = 0.2 W. For a 70-kg (150-lb) person, an integral dose value of E_{tot} = 1 J corresponds to an "average whole body dose" of about 1 J ÷ 70 kg = 0.014 Gy = 14 mGy.

2.D. FREE-IN-AIR EQUILIBRIUM DOSE-PITCH PRODUCT

During acceptance tests (see section 3 for materials, equipment—e.g., ionization chamber in section 3.C—and instructions to be applied in the measurements), it is useful to determine values of the equilibrium dose-pitch product free-in-air, $\hat{D}_{eq,air}$:

$$\hat{D}_{eq,air} = \frac{1}{nT}\int_{-\infty}^{\infty} f_{air}\left(z'\right)dz' \approx \frac{a}{nT} f_{air}\left(z=0\right), \tag{14}$$

where $f_{air}(z)$ is the associated dose profile free-in-air resulting from a single axial rotation centered about the central scan plane (z = 0); see Eqs. (3)–(5) and Fig. 1. $\hat{D}_{eq,air}$, like its in-phantom counterpart $\hat{D}_{eq}$, is directly proportional to the same over-beaming factor $a/(nT)$, and it is also proportional to the machine output $f_{air}(0)$ along the central ray z = 0. As there is minimal radiation scatter free-in-air, $f_{air}(z)$ can be identified with the primary-radiation component: $f_{air}(z) \approx f_{p,air}(z)$. Values of $\hat{D}_{eq,air}$ that are initially measured can subsequently be checked in routine quality control testing of the constancy of x-ray emissions. They can also be used to establish phantom-to-air ratios $\left[\hat{D}_{eq}/\hat{D}_{eq,air}\right]$ at acceptance to which subsequent measurements of $\hat{D}_{eq,air}$ could be applied to infer in-phantom equilibrium dose-pitch products $\hat{D}_{eq}$. The ratios $\left[\hat{D}_{eq}/\hat{D}_{eq,air}\right]$ are analogous to "phantom factors" that have been demonstrated to vary significantly amongst scanner models.[39]

3. MEASUREMENT OBJECTIVE, MATERIALS, EQUIPMENT, AND INSTRUCTIONS

3.A. OBJECTIVE

For each clinically relevant mode of CT operation—helical, axial, fluoroscopic, or cone-beam scanning—and for each clinically relevant set of operating conditions {focal spot size, bow-tie filter, kVp, n, T, (a)[15]}, the objective is to evaluate

(1) the equilibrium dose-pitch product $\hat{D}_{eq}$ for modes involving table translation and the single-scan dose $f(0)$ for stationary-table modes[16]—each dose metric normalized per mAs per rotation—on the central axis and on a peripheral axis of cylindrical phantoms, and

(2) corresponding quantities free-in-air.

Such evaluation constitutes a reasonable characterization of CT dose for the purposes of acceptance testing and quality control.

For any particular set of operating conditions, a single assessment of the equilibrium dose constant $(b/a) \cdot D_{eq}$ can be used to reduce the number of measurements required to evaluate $\hat{D}_{eq}$ for the other sets of operating conditions.[23] In phantoms, these parameters can be evaluated from measurements and analyses made via an approach-to-equilibrium function $h(L)$.

3.B. PHANTOMS

While this report describes a new CT dosimetry system that depends crucially on radiation absorption and scattering phantoms sufficiently long (e.g., at least 45 cm) to accommodate scanning lengths L_{eq} related to cumulative dose equilibrium, at this time there is not consensus to recommend precise specifications for

- phantom material composition
- phantom dimensions and shape (e.g., elliptical cylinders, or other shapes that are not right circular cylinders to probe CT modes of operation using tube current modulation or other means of automatic exposure control)
- media to which reported dose values would refer (i.e., dose in air of an ionization chamber located within the phantom material vs. dose in the phantom material itself)

---

[15] In keeping track of the number of different operating conditions for which measurements are to be made, it is assumed that each unique combination of n and T is associated with one and only one value of the collimation width a. For example, for GE LightSpeed scanners employing a small focal spot, when $n = 4$ and $T = 2.5$ mm ($nT = 10$ mm), $a = 11.4$ mm ± 1.3%, and there is no other value of a associated with that particular combination of n and T.[23] Another example: when $n = 8$ and $T = 1.25$ mm ($nT = 10$ mm), $a = 12.0$ mm exclusively.[23] However, any particular value of a may correspond to *more* than one combination of n and T. For example, for GE LightSpeed scanners employing a small focal spot, the collimation width of $a = 12.0$ mm is associated with $n = 8$ and $T = 1.25$ mm ($nT = 10$ mm), and it is also associated with $n = 16$ and $T = 0.625$ mm ($nT = 10$ mm).[23]

[16] In a scanning mode involving fan-beam or cone-beam irradiation without translation of the patient table, the clinically relevant in-phantom dose descriptor is $f(0)$, not $\hat{D}_{eq}$.

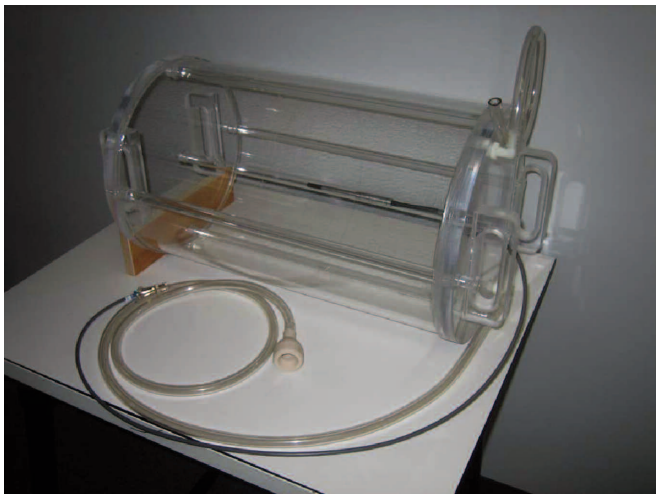

Figure 4. Quick-fill water phantom: 30-cm diameter, 50 cm long body phantom with quick-disconnect hoses for attaching to a small centrifugal pump. A Farmer chamber is shown on the central axis.

- values of ratios of mass energy-absorption coefficients of the phantom material vs. air, for the purpose of evaluating dose in the phantom material
- how many phantoms (i.e., corresponding, for example, to an adult-size torso, head, pediatric-size torsos and heads) would be sufficient to represent the attenuation characteristics of the clinical population in a way reasonable and practicable for purposes of dosimetric acceptance testing and quality control.

We recommend the formation of a new task group to address these particular points and related issues. The following examples illustrate the kinds of phantoms that merit consideration:

3.B.1. Water

A water-filled, 30-cm diameter phantom, 50 cm long (Fig. 4) would correspond to the attenuation and absorption of the average-sized adult body.[40] The phantom is designed to be transported empty, and once placed on the table, it can be quickly filled or emptied in 2 minutes with a small pump operating from a room sink as a reservoir. A second water-filled phantom, of 20-cm diameter, could be used to correspond to the attenuation properties of an adult head and pediatric body.

3.B.2. Polyethylene (PE)

Monte Carlo calculations[17] suggest that PE cylinders with diameters approximately 3.5 cm larger than those of water cylinders would yield values of dose in air (at the phantom center, i.e., in an ionization chamber) that match the corresponding values of dose in air for the water phantoms. When one considers central doses in the respective media rather than dose in air, the central dose in PE of 25-cm diameter would be approximately the same as the central dose in a water

[17] J.M. Boone, *A Short Report for CT Physicists on the Equivalency between Water and Polyethylene in CT Dosimetry*, private communication to AAPM TG-111, November 2, 2008.

cylinder of 26-cm diameter; for a 30-cm diameter phantom, the dose in PE would be nearly the same as the dose in water. The explanation of the seeming paradox in the matching of dose values for the respective media at a particular diameter without matching of central air dose values has to do with the difference in ratios of the spectrally averaged mass energy-absorption coefficients for the medium with respect to that for air, where this ratio is denoted by the symbol $\left(\bar{\mu}_{en}/\rho\right)_{air}^{material}$. For polyethylene, $\left(\bar{\mu}_{en}/\rho\right)_{air}^{PE} \sim 0.78$ is lower than that of water, where $\left(\bar{\mu}_{en}/\rho\right)_{air}^{water} \sim 1.09$.[41] Hence, because the dose is reduced (per unit air dose in the center) by a factor ~ 0.78, the diameter of a polyethylene cylinder would need to be somewhat smaller than that of a water cylinder in order to compensate so as to yield the same value of *in-medium* dose. For the purpose of measurements of equilibrium dose, 30-cm long modules of PE cylinders could be assembled adjacent to each other along the longitudinal axis.

3.B.3. Polymethyl methacrylate (PMMA)

While dose in a 32-cm diameter PMMA phantom would be approximately 30% lower than the dose in a 30-cm diameter water cylinder,[41] there is a large stock of PMMA phantoms already in use in the field, and such phantoms could be assembled contiguously for requisite lengths. Dose in 16-cm diameter PMMA would be relatively close to the value in a 20-cm cylinder of water.[41]

3.C. IONIZATION CHAMBER AND ELECTROMETER

The measurements described in this report should be made using a conventional thimble ionization chamber with an active length l of 20–35 mm for charge collection, a nominal collection volume of at least 0.6 cm^3, a flat energy response (~1.5% variation) over the half-value layer (HVL) range 2–15 mm Al,[25] and which is calibrated by an accredited dosimetry calibration laboratory (ADCL) for ranges of beam quality and kVp (80–140 kVp) associated with those of CT scanner spectra. An example of such a chamber is shown in Fig. 5.

Figure 5. RadCal "Farmer-type" 0.6-cm^3 ionization chamber and cable. The red line along the circumference of the chamber locates the middle of the charge-collection volume.

Depending on the particular electrometer, it may be important for the ionization chamber to be configured with a cable long enough to allow the electrometer to operate out of the phantom scatter-radiation field, e.g., shielded in the control area outside the scan room, in order to avoid induction of extra-cameral currents[18] in the electrometer itself;[27] not to mention the increase in data collection efficiency obtained by locating the electrometer at the CT control console. If the chamber is only equipped with a short cable, an extender cable could be used,[19] or alternatively the electrometer can be shielded with a lead apron. The electrometer should provide a bias voltage of at least ±300 volts, and it should have sensitivity and a leakage current consistent with the ionization chamber volume and dose rate. Since measurements involve irradiation of the entire ionization chamber stem plus a significant length of cable, the ionization chamber should be tested for a "stem effect" prior to use.[27] A 0.6-cubic centimeter Farmer-type ionization chamber satisfies all of these criteria,[18,19,25,27] but other types may be equally satisfactory. At least one such 0.6-cm^3 Farmer-type chamber is available for dosimetric electrometers used by diagnostic physicists, and it has been found to exhibit good performance, comparable to that of the Nuclear Enterprise 2571 Farmer-type chamber.

If q (nC) is the total charge collected by the ionization chamber during scanning over the length L, and N_k (mGy/nC) is the ionization chamber calibration factor supplied by an ADCL, then under the assumption that the chamber reading q has been corrected for temperature and pressure, the dose to the phantom material (e.g., water, PE, or PMMA) is given by

$$D_{material} \approx K_a \left(\bar{\mu}_{en}/\rho\right)_{air}^{material} \approx qN_k \left(\bar{\mu}_{en}/\rho\right)_{air}^{material}, \tag{15}$$

where $K_a \approx qN_k$ approximates (to within ~2% for the range of beam quality of CT systems) the magnitude of the air kerma in the cavity occupied by the ionization chamber,[27,42,43] and $\left(\bar{\mu}_{en}/\rho\right)_{air}^{material}$ is the ratio of the spectrally averaged mass energy-absorption coefficient of the phantom material to that of air. (Note that if the dosimetric reference medium were designated to be air itself, then the value of this ratio would be unity.) This ratio $\left(\bar{\mu}_{en}/\rho\right)_{air}^{material}$ will vary somewhat with kVp, with the shaped filtration, with the phantom, between the central and peripheral axes in a given phantom,[44] and even as the ionization chamber moves along the z-axis. However, the variation is less than 3%. For water, 120-kVp–based estimates for the average $\left(\bar{\mu}_{en}/\rho\right)_{air}^{water}$ are ~1.06[4] to ~1.09[41]. For PE and PMMA, estimates of $\left(\bar{\mu}_{en}/\rho\right)_{air}^{PE}$ and $\left(\bar{\mu}_{en}/\rho\right)_{air}^{PMMA}$ are 0.78 and 0.87, respectively.[41] For any particular medium, a more detailed

[18] Unshielded electronic components may be susceptible to such spurious currents: for these x-ray energies, any p-n junction—even unbiased—acts like an ionization chamber because of the junction potential and has a sensitivity more than four orders of magnitude higher than that of an air-filled ionization chamber of the same volume. In this application the ion chamber is integrating very low currents when traversing the scatter tails of the dose profile (unlike the typical diagnostic application using a large volume ion chamber in the unattenuated primary beam). The prudent physicist will therefore perform a simple verification (perhaps with a lead apron) under the above experimental conditions to rule out such errors (in lieu of relying solely on the manufacturer's assurance).

[19] An extender cable could possibly introduce signal degradation and noise pick-up; however, a simple test with and without the extender cable should verify its suitability. The physicist should carefully consider the strengths and limitations of the particular equipment when configuring the components—ionization chamber, cable, electrometer—for measurements.

analysis of the variation with kVp and HVL is warranted to develop estimates of mass energy-absorption coefficient ratios more precisely matched to x-ray energies and beam quality.

3.D. MEASUREMENT INSTRUCTIONS

3.D.1. Select CT conditions of operation

While equilibrium doses and stationary-table, single-scan central doses are to be evaluated for each clinically relevant set of operating conditions {*focal spot size, bow-tie filter,*[20] *kVp, n, T, a*}, for each iteration through the instructions, start by designating a "reference" set of operating conditions $\{...\}_{ref}$ to be associated with doses denoted $D_{eq,ref}$ and $f_{ref}(0)$, with parameters *focal spot size*$_{ref}$, *bow-tie filter*$_{ref}$, n_{ref}, T_{ref}, a_{ref}, b_{ref}, p_{ref}, etc., and with an approach-to-equilibrium function denoted $h_{ref}(L)$. We recommend that for the initial designation, the reference set of operating conditions correspond to those of the most frequently used clinical protocol, for example, {large focal spot, body bow-tie filter, kVp_{ref} = 120 kVp, n_{ref} = 4 slices per scan, T_{ref} = 5-mm thickness per slice}$_{ref}$. If at all possible, select a combination of n_{ref} and T_{ref} that corresponds to a value of the pre-patient collimation projection width a_{ref} that is known *a priori* (via direct measurement with film, with an OSL imager, or via the manufacturer) or can be inferred with Eq. (7).

For normalization to the tube current-time product, e.g., to 100 mAs per rotation, in scanning a phantom, select a value large enough, such as 400 mAs, so that the signal/noise ratio within the $f(z)$ dose profile tails at the level of 1% peak signal assures that dose values accrued in the tails during scanning are statistically significant. It should be understood that dose metrics to be evaluated, $\hat{D}_{eq}$ and $f(0)$, refer to values that are normalized to the current-time product, e.g., to 100 mAs per rotation.

3.D.2. Set up the phantom and ionization chamber

Place the thimble ionization chamber in the phantom central hole. Center the charge-collection volume of the chamber at the phantom central plane, which will correspond to the midpoint (z = 0) of the scanning range ($-L/2$, $L/2$) for all measurements. Align the phantom central axis with the scanner axis of rotation. See Fig. 6.

3.D.3. Select *b, n, T,* and *p* for table translation

In subsequent measurements for scanning modes involving table translation, although either helical or axial scanning can be used for most measurements, helical scanning is relatively more convenient than axial scanning. For helical-scanning data to be acquired on the phantom central axis, dose would be a smooth function of z, and therefore any value of pitch could be selected; p = 1 is a reasonable default value. For helical scanning on peripheral axes however, and also for axial scanning on any axis where there is table translation, as the dose along z would be oscillatory, quasi-periodic with period b, the pitch should be small enough so that oscillations would be averaged out over the active length l of the ionization chamber: $b < l$, i.e., $p < l/(nT)$.[28] If possible, use $b \leq l/2$, i.e., $p \leq l/(2nT)$, which allows for averaging over at least two oscillations

[20] The bow-tie filter selected should correspond to the phantom size (i.e., representing adult or pediatric torso or head) and be appropriate for the clinical protocol associated with the other parameters of the technique set.

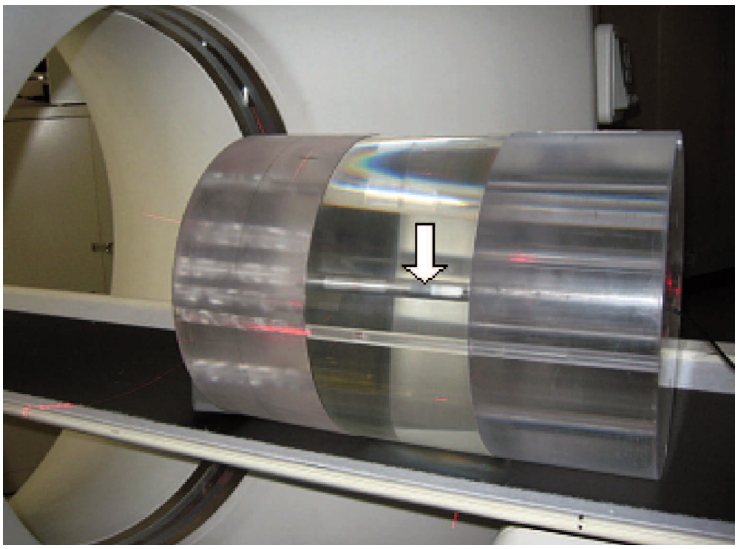

Figure 6. The 0.6-cm^3 ionization chamber (indicated by the arrow) is shown with the middle of its charge-collection volume positioned at the center of the phantom assembly and aligned along the scanner axis of rotation (z-axis direction). The phantom assembly shown comprises three adjacent PMMA sections, each 15-cm long and of 32-cm diameter, assembled along the patient table and held together with filler rods in mutually aligned holes. Overall length of the assembled phantom is 45 cm.

and reduces the amplitude of oscillation typically to less than ~10%. For the 0.6-cm^3 Farmer chamber, $l \approx 23$ mm, and thus for $nT = 20$ mm, $p \approx 0.5$ is a good selection.

The adequacy and robustness of this method on the peripheral axes in the PMMA body phantom has been experimentally demonstrated for total nominal tomographic section widths nT up to 40 mm.[27] If the collimation widths a are known, then the value of $D_{eq,\,peri}$ on the peripheral axis for a total section width $nT \geq 40$ mm can be inferred from the constancy of $(b/a) \cdot D_{eq,\,peri}$—cf. Eq. (6)—and from a value $D_{eq,\,peri}$ measured with $nT < 40$ mm. If the collimation widths a are not known, and if a suitably small value of pitch cannot be selected to accommodate averaging over the short active length of the thimble chamber, an approximate value for $\hat{D}_{eq,peri} \equiv pD_{eq,peri}$ may be inferred as follows:

$$p_1 D_{eq,peri,\,nT\geq 40\text{ mm}} \approx p_1 D_{eq,cen,\,nT\geq 40\text{ mm}} \times \left(\frac{p_2 D_{eq,peri,\,nT<40\text{ mm}}}{p_2 D_{eq,cen,\,nT<40\text{ mm}}} \right). \tag{16}$$

In Eq. (16), $D_{eq,\,cen,\,nT\geq 40\text{ mm}}$ is the value of the equilibrium dose measured on the phantom central axis for a particular $nT \geq 40$ mm (i.e., which corresponds to one particular value of a) where there is no restriction on selected pitch (say p_1) even for the relatively large (≥ 40 mm) value of nT. However, values for equilibrium doses in the ratio in Eq. (16) are each measured for a narrower width $nT < 40$ mm with a pitch value p_2 that satisfies the condition $p_2 < l\,/(nT)$.[21]

[21] Because the equilibrium dose-pitch product is independent of pitch, the numerator and the denominator of the ratio in Eq. (16) can each be evaluated at different values of pitch (say p_2 and p_3) so long as the scanning in each case is done with the same value of nT (< 40 mm) corresponding to one particular value of a.

3.D.4. Scan, measure, and record cumulative dose values $D_L(0)$

For scanning modes involving table translation, for the selected set of operating conditions, pitch, and related parameters, and for a group of scanning lengths ranging from L = 50 mm to L = the phantom length minus nT,[22] begin the measurement set with scans along the phantom central axis. For each value of L used, evaluate a cumulative central dose $D_L(0)$ defined in Eq. (2). Values of $D_L(0)$ are determined according to Eq. (15) via measurements of the ionization chamber air kerma. Figs. 7a–c illustrate schematically a sequence of measurements of $D_L(0)$ values. For simplicity and clarity of presentation, only three scanning lengths are depicted, and the components within the figures are not drawn to scale: in actual measurements, the full length of the thimble ionization chamber would be irradiated in each of the scanning sequences.

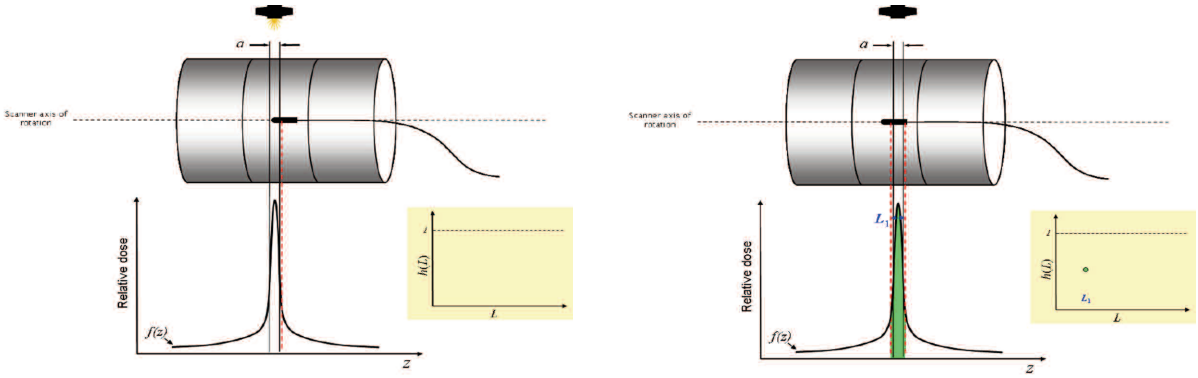

Figure 7a. (Left figure) Phantom assembly and centered ionization chamber moving together from right to left over scanning length L_1 (right figure), so that the chamber integrates values over the area indicated in green under the dose profile.

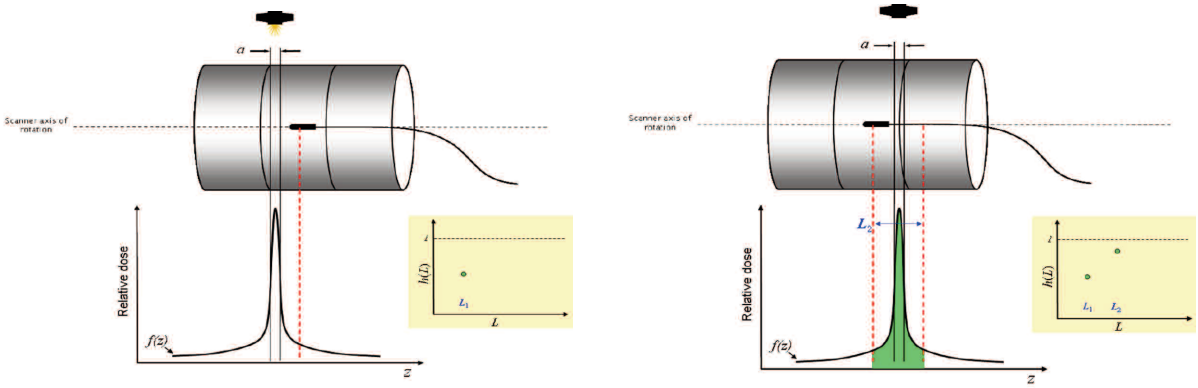

Figure 7b. (Left figure) Phantom assembly and centered ionization chamber moving together from right to left over scanning length L_2 (right figure), so that the chamber integrates values over the area indicated in green under the dose profile.

[22] It is prudent to limit the maximum scanning length L to a value slightly less than the phantom length in order to prevent the primary beam from extending beyond the end of the phantom and impinging directly on the ion chamber cable during charge collection in the low-amplitude scatter tails at the opposite end. In no case should the scanning length L be taken to have a value greater than the phantom length.

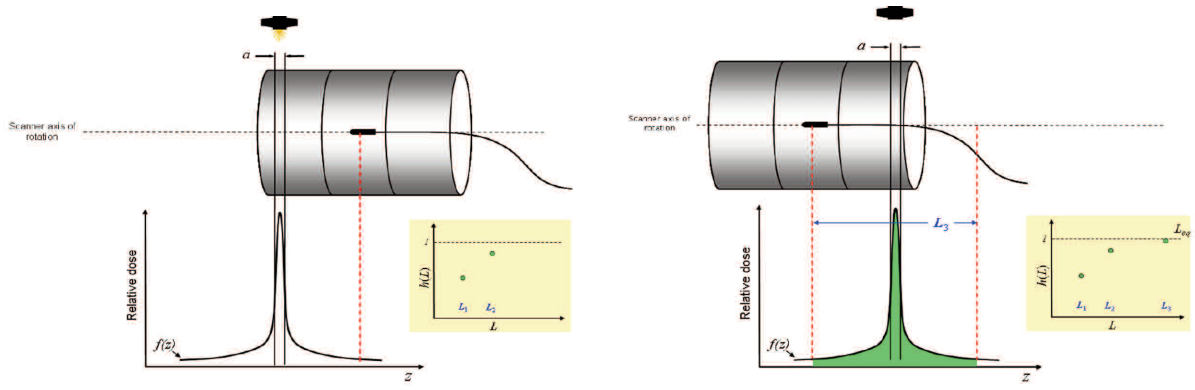

Figure 7c. (Left figure) Phantom assembly and centered ionization chamber moving together from right to left over scanning length L_3 (right figure), so that the chamber integrates values over the area indicated in green under the dose profile.

When determining a value for L, note that in helical scanning, because scanners use over-ranging to accommodate interpolation and reconstruction algorithms, the programmed scanning length *per se* or the total length along z of reconstructed tomographic sections does not correspond to the actual scanning length L.[45] For dosimetry measurements the actual scanning length L, which includes any over-ranging in helical scanning, should be quantified according to the relation $L = vt$ for helical scanning modes. In this expression for L, $v = b/\tau$ is the table velocity, $b = pnT$ the table increment per rotation, τ the rotation period, and t the total beam "on-time" ("loading time") during scanning over length L. In some scanners, t may be indicated when the scanning protocol has been selected; following scanning over a selected range, the post-exposure on-time t may be indicated directly, or a post-exposure value of mAs may be indicated from which t may be inferred as $t = mAs/mA$. If no indication is available from which t may be determined, L may be estimated as the sum of the programmed scanning range plus an over-ranging increment ΔL, where, for a given set of conditions of operation, ΔL is the ratio of the intercept to the slope of a plot of free-in-air kerma values versus programmed scanning lengths.[45] If axial scanning is done, $L = Nb$, where N is the number of rotations.

3.D.5. Evaluate and record the equilibrium dose D_{eq}

For scanning modes involving table translation and for the CT conditions of operation selected in 3.D.1, mathematically fit the values of $D_L(0)$ measured in 3.D.4 with Eqs. (8) and (9), i.e., applying the "approach-to-equilibrium" function $h(L)$, in order to estimate values for the equilibrium dose D_{eq}, the equilibrium scanning length L_{eq}, and the third fit parameter (α). (See Fig. 3 and reference 27.) Values of L_{eq} and α yield the approach-to-equilibrium function $h(L)$ defined according to Eq. (9). Compute and record the equilibrium dose-pitch product $\hat{D}_{eq} \equiv pD_{eq}$, where p is the pitch used in acquiring $D_L(0)$ values. If the pre-patient collimation projection width a associated with this acquisition is known, also compute and record the equilibrium-dose constant $(b/a) \cdot D_{eq}$, which is independent of the collimation width a and the table interval b.

3.D.6. For CT modes with table translation, evaluate and record the equilibrium dose-pitch product $\hat{D}_{eq}$

Retaining the same $filter_{ref}$ and kVp_{ref} designated in 3.D.1, systematically permute the respective values of *focal spot size*, n, and T. For each clinically relevant combination {*focal spot size, n, T*}, if the scanning mode involves table translation, evaluate $\hat{D}_{eq}$ as described in either of the following paragraphs: (a) or (b). On the basis of the definition of $h(L)$ in Eq. (9), and from the weak dependence of $h(L)$ on a,[15] it can be assumed that the same approach-to-equilibrium function evaluated in 3.D.5 is valid here as well, and there is no need to re-evaluate it in 3.D.6.

(a) If the value of the collimation width a associated with a particular combination {*focal spot size,* n_a, T_a} is known, then the equilibrium dose-pitch product $\hat{D}_{eq}(a)$ can be inferred by scaling the equilibrium-dose constant $(b_{ref}/a_{ref})D_{eq,ref}$ obtained at the reference values of a_{ref} and $n_{ref}T_{ref}$ in 3.D.5 to any other values of (a, n_aT_a), using the scaling factor $a/(n_aT_a)$:

$$\hat{D}_{eq}(a) = \left(\frac{a}{n_a T_a}\right) \cdot \left(\frac{b_{ref}}{a_{ref}}\right) \cdot D_{eq,ref}\left(a_{ref}\right). \tag{17}$$

Here n_aT_a is the nominal total width of the tomographic sections for acquisitions associated with collimation width a. In other words, if the value of a is known for each associated combination {*focal spot size, n, T*}, then each of the respectively associated values $\hat{D}_{eq}(a) \equiv pD_{eq}(a,p)$ can be determined via Eq. (17) without additional measurements.[23,27]

(b) If the value a associated with a particular combination {*focal spot size, n, T*} of operating conditions is not known, repeat instructions 3.D.3 and 3.D.4 for that combination, but only for a single scanning length $L \geq L_{eq}$, where L_{eq} is the value estimated according to 3.D.5. With this scanning length, the measured cumulative dose is the equilibrium dose D_{eq}, and for the pitch p selected for this scanning, the equilibrium dose-pitch product $\hat{D}_{eq}$ is just pD_{eq}.

3.D.7. For CT modes without table translation, evaluate and record the single-scan central dose $f(0)$

For scanning modes that do not involve table translation but nevertheless apply the same CT conditions of operation selected in 3.D.1 that were used to evaluate {α, L_{eq}, D_{eq}} in 3.D.5, measure $f_{ref}(0)$ directly with the smallest charge-collection-length (l) ionization chamber consistent with the condition that $l < n_{ref}T_{ref}$.

Then, retaining the same $filter_{ref}$ and kVp_{ref} designated in 3.D.1, systematically permute the respective values of *focal spot size*, n, and T. For each collimation width a associated with a particular clinically relevant combination {*focal spot size, n, T*}, measure $f_a(0)$ directly with the smallest charge-collection-length (l) ionization chamber consistent with the condition that $l < nT$.

3.D.8. Repeat 3.D.1 through 3.D.7 for each other clinically relevant combination of *bow-tie filter* and *kVp*

3.D.9. Repeat 3.D.1 through 3.D.8 for peripheral-axis scanning

In iterating through instruction 3.D.2 for peripheral-axis scanning, center the thimble ionization chamber at the phantom central plane in a peripheral hole. Align the phantom central axis with the scanner axis of rotation. Rotate the phantom about its central axis so that the peripheral hole containing the ionization chamber is in the 12 o'clock position, i.e., directly above the scanner axis of rotation.

3.D.10. Repeat 3.D.1 through 3.D.9 with each different-sized phantom

3.D.11. Measure and record equilibrium dose-pitch products $\hat{D}_{eq,air}$ free-in-air

For each clinically relevant set of operating conditions {*focal spot size, filter, kVp, n, T*}, evaluate $\hat{D}_{eq,air}$ as follows:

(a) As in 3.D.1, designate a "reference" set of conditions of operation and related parameters to be associated with the initial iteration of free-in-air measurements. Since for all practical purposes free-in-air dose profiles do not manifest radiation-scatter tails, select any convenient *mAs* per rotation for purposes of dose normalization per *mAs*.

(b) Clamp or otherwise fix the base of the same thimble ionization chamber used for phantom measurements to a sufficiently long extender rod (e.g., using plastic "tie wraps" to attach the chamber base to a thin wooden dowel), where the rod may be attached to a laboratory stand such that it moves longitudinally with the table, and such that the sensitive volume is always located far enough from any structure, particularly from the patient support table itself, to reduce scattered radiation. Align the chamber axis parallel to the z-axis on the axis of rotation. See Fig. 8.

(c) For a "generalized pitch"—defined in Eq. (4)—with value $p = 1$, perform either helical or axial scanning and translate the ionization chamber so that the chamber starts entirely outside the beam, passes through the beam, and then finishes entirely beyond the other side of the beam.[23] A conservative operational value for the scanning length would be $L = l + nT + 15$ mm. This procedure is tantamount to measuring the total area, i.e., its infinite integral, under the free-in-air dose profile, an example of which is depicted in Fig. 1. If a pitch value p other than 1 is used, note the value of the pitch and apply it in the following instruction (d).

[23] In a helical-scanning mode, the ionization chamber would be translated in a continuous movement through the scan plane a total distance L during tube rotations and irradiation. In an axial-scanning mode, the ionization chamber would be moved through the scan plane in successive translational steps (between rotations and irradiation) a total distance L.

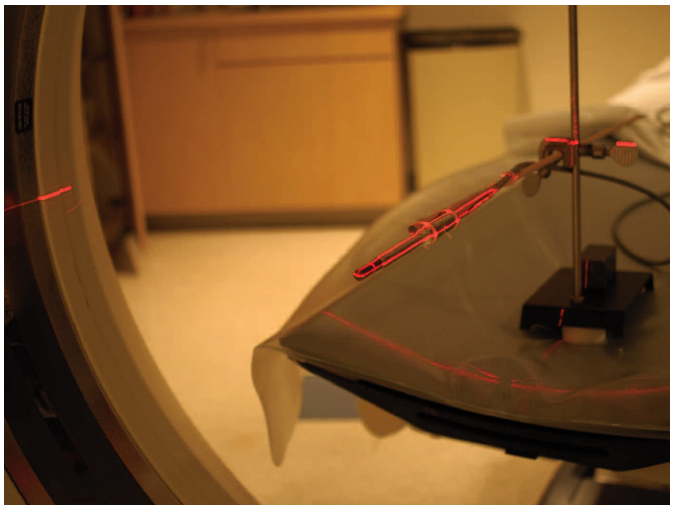

Figure 8. Thimble ionization chamber free-in-air and aligned along the axis of rotation. The chamber is attached to an extender rod from a lab stand, and the assembly is illuminated by the CT system alignment laser lights.

(d) Do the scanning and measurement, and, according to Eqs. (15) and (14), evaluate the equilibrium dose in terms of the air kerma measured, i.e., $D_{eq,air} \approx qN_k$. The equilibrium dose-pitch product $\hat{D}_{eq,air}$ is then just equal to $D_{eq,air}$ for $p = 1$, and for $p \neq 1$ the equilibrium dose-pitch product $\hat{D}_{eq,air}$ is just equal to $pD_{eq,air}$.

(e) Retaining the same *filter* and *kVp* selected in the instruction (a) of 3.D.11 (where the "reference" conditions are designated), systematically permute the respective values of *focal spot size*, *n*, and *T*. For each clinically relevant combination {*focal spot size, n, T*}, evaluate $\hat{D}_{eq,air}$ in a manner analogous to that of 3.D.6: if collimation width *a* is known for a particular combination {*focal spot size, n, T*}, use Eq. (17) to evaluate $\hat{D}_{eq,air}(a)$ from the previously determined product $(b_{ref}/a_{ref}) \cdot D_{eq,air,ref}(a_{ref})$. If collimation width *a* is not known, measure $\hat{D}_{eq,air}$ as prescribed by instructions (b), (c), and (d) of 3.D.11.

(f) Repeat the preceding instructions (a) through (e) of 3.D.11 for each other clinically relevant combination of *filter* and *kVp*. For each iteration of instruction (a), re-designate as "$filter_{ref}$" and "kVp_{ref}" each clinically relevant permutation of *filter* and *kVp*, respectively.

(g) Repeat instructions (a) through (f) of 3.D.11 with the ionization chamber placed at the same radial location it had occupied for measurements along the peripheral axis of each phantom used. For a phantom of radius *R*, the measurement location corresponding to the phantom peripheral axis is at a distance of $R - 10$ mm above the axis of rotation. For peripheral-axis scanning free-in-air, use the same small pitch values $p \leq l/(2nT)$ as were used for the in-phantom measurements (cf. 3.D.3).

4. GLOSSARY

a — Width (mm, along the axis of rotation) of the pre-patient z-axis collimator geometrically projected from the centroid of the x-ray source. Parameter a corresponds to the full-width at half-$f_p(0)$ of the primary-beam dose profile $f_p(z)$.[23,27] In the text, "collimation width" is used interchangeably with "a" and refers to a geometric projection on the axis of rotation.

α — Fit parameter (dimensionless) associated with the magnitude of the exponential term in the approach-to-equilibrium function $h(L)$; $0 \leq \alpha \leq 1$. For $\alpha = 1$, scattering contributions dominate; for $\alpha = 0$, primary-radiation contributions dominate. See Eqs. (8) and (9).

b — Scan interval (mm). In axial scanning, b is the midpoint-to-midpoint spacing between successive scans. In helical scanning, b is the distance the table moves continuously at constant velocity v per rotation period τ: $b = v\tau$, the table advance per rotation.

$(b/a) \cdot D_{eq}$ — Equilibrium dose constant, a parameterization of the equilibrium dose (mGy), where D_{eq} is the equilibrium dose evaluated at collimation width a and scan interval b. Since D_{eq} is directly proportional to a and inversely proportional to b, the product $(b/a) \cdot D_{eq}$ is independent of a and b. See Eq. (6).

D_{eq} — Equilibrium dose (mGy) accumulated at longitudinal position $z = 0$, viz., at the midpoint of a scanning range sufficiently long so that radiation from the "scatter tails" of outlying scan sections is sufficiently remote to make negligibly small additional contributions toward the accrual of dose. For scanning at pitch $p = b/(nT)$, $D_{eq} \propto a/b = a/(pnT)$, i.e., the equilibrium dose is directly proportional to the collimation width a and inversely proportional to the scan interval b, i.e., inversely proportional to the pitch p. See Eqs. (3), (8), and (9).

$\bar{D}_{eq}$ — Equilibrium dose $D_{eq}(r)$ average (mGy) over the area πR^2 of the central ($z = 0$) scan plane in a phantom of radius R. See Eq. (13).

$\hat{D}_{eq}$ — Equilibrium dose-pitch product (mGy), pD_{eq}, where D_{eq} is the equilibrium dose evaluated at pitch p. Since D_{eq} is inversely proportional to p, the product pD_{eq} is independent of p. See Eq. (5).

$D_L(z)$ — Cumulative dose (mGy) at longitudinal position z resulting from scanning over a range L. See Eq. (1).

$D_L(0)$ — Cumulative dose (mGy) at longitudinal position $z = 0$, viz., at the midpoint (central plane) of a scanning range of length L. See Eq. (2).

$D_N(z)$ — Cumulative dose (mGy) at longitudinal position z resulting from scanning with N rotations done without table translation. See Eq. (10).

$D_N(0)$ — Cumulative dose (mGy) at longitudinal position $z = 0$, viz., at the central plane of the scanner in scanning with N rotations done without table translation. See Eq. (11).

E_{tot} Integral dose, i.e., the total energy (J) absorbed in the phantom, a simplified indicator of radiation risk for a patient. See Eqs. (12) and (13).

$f(z)$ Single-scan dose (mGy) at longitudinal position z, where the table is stationary. $f(z)$ is comprised of a component $f_p(z)$ associated with primary radiation plus a component $f_s(z)$ associated with scatter radiation. The collection of $f(z)$ values for a single axial scan is referred to as the "dose profile." It is assumed that $f(z)$ is a symmetric function and that $f(0)$, the midpoint value, is the peak value.

$h(L)$ Approach-to-equilibrium function (dimensionless), an empirically derived expression characterizing the dependence on scanning length L of the ratio of the central-plane cumulative dose $D_L(0)$ to the equilibrium dose D_{eq}. See Eqs. (8) and (9).

K_a Air kerma (mGy).

l Charge-collection length (mm) of an ionization chamber.

L Scanning length (mm), i.e., the distance through which the dose profile $f(z)$ is translated during a sequence of scanning. For axial scanning, $L = Nb$; for helical scanning, $L = vt$; for scanning without longitudinal translation of the table, $L = 0$.

L_{eq} "Equilibrium" scanning length, a *finite* scanning length for which $D_{Leq}(z = 0)$ is arbitrarily close to the value D_{eq}, i.e., a scanning length with respect to which scanning of a longer range makes for practical purposes a negligibly small difference in the estimation of the equilibrium dose. In this report L_{eq} is evaluated as a fit parameter (mm) corresponding to a scanning length characteristic of exponential saturation in the approach-to-equilibrium function: by convention, L_{eq} is identified as the value of the scanning length L for which $\exp(-4L/L_{eq}) = \exp(-4) \approx 0.0183$. See Eqs. (8) and (9).

$\left(\bar{\mu}_{en}/\rho\right)_{air}^{material}$ Ratio (dimensionless) of the spectrally averaged mass energy-absorption coefficient of the phantom material to that of air.

n Number (dimensionless) of tomographic sections acquired simultaneously in a single scan.

N Number (dimensionless) of rotations of the x-ray tube associated with a sequence of scanning over a range L, where N may not be an integer for helical scanning.

N_k Ionization chamber calibration factor in terms of air kerma per collection charge (mGy/nC) supplied by an accredited dosimetry calibration laboratory.

nT Total nominal width (mm) of the reconstructed tomographic sections acquired in a single scan.

p The "generalized" pitch (dimensionless), i.e., associated with either axial or helical scanning. The pitch is the ratio of the scan interval b to the total nominal width nT of reconstructed tomographic sections acquired simultaneously per single scan. See Eq. (4).

q	Total charge (nC) collected by the ionization chamber during scanning over the length L. See Eq. (15).
r	Radial coordinate (mm). $r = 0$ locates the scanner axis of rotation and the central axis of a phantom aligned along the axis of rotation. See Eqs. (12) and (13).
R	The radius (mm) of a phantom shaped as a right-circular cylinder. See Eqs. (12) and (13).
ρ	Uniform mass density (kg/m^3) of a phantom. See Eqs. (12) and (13).
t	Total irradiation time (s), also referred to as the beam "on-time" or x-ray tube "loading-time," in a sequence of scanning.
T	Nominal width (mm) of a single tomographic section.
τ	Period (s) of rotation of the x-ray source over 2π about the axis of rotation.
v	Constant table velocity (mm/s) in a sequence of helical scanning.
z	Longitudinal coordinate (mm). $z = 0$ locates the central plane, i.e., the midpoint in a range of scanning over length L. For scanning without table translation, $z = 0$ locates central plane of the scanner.

REFERENCES

1 Shope, T., R. Gagne, and G. Johnson. (1981). "A method for describing the doses delivered by transmission x-ray computed tomography." *Med Phys* 8:488–495.

2 U.S. Food and Drug Administration. "Diagnostic X-Ray Systems and Their Major Components; Amendments to Performance Standard. Final rule." *Federal Register* 49 (171), 34698-34714 (August 31, 1984); "Computed tomography (CT) equipment," *Code of Federal Regulations,* 4-1-08 Edition, Title 21, Part 1020, Section 33, pp. 646–651, (Washington, D.C., 2008); U.S. Food and Drug Administration, Guidance for Industry, FDA Staff and Third Parties - Provision for Alternate Measure of the Computed Tomography Dose Index (CTDI) to Assure Compliance with the Dose Information Requirements of the Federal Performance Standard for Computed Tomography, http://www.fda.gov/cdrh/ocer/guidance/1609.html, (October 20, 2006).

3 Leitz, W., B. Axelson, and G. Szendro. (1995). "Computed tomography dose assessment—a practical approach." *Radiat Prot Dosimetry* 57:377–380.

4 Jessen, K. A. , P. C. Shrimpton, J. Geleijns, W. Panzer, G. Tosi. (1999). "Dosimetry for optimization of patient protection in computed tomography." *Appl Radiat Isot* 50:165–172.

5 International Standard IEC 61223-3-5, Evaluation and routine testing in medical imaging departments—Part 3-5: Acceptance tests—Imaging performance of computed tomography X-ray equipment, First edition (International Electrotechnical Commission, Geneva, Switzerland, 2004); Corrigendum 1 (2006).

6 International Standard IEC 61223-2-6, Evaluation and routine testing in medical imaging departments—Part 2-6: Constancy tests—Imaging performance of computed tomography X-ray equipment, Second edition (International Electrotechnical Commission, Geneva, Switzerland, 2006).

7 International Standard IEC 60601-2-44, Medical Electrical Equipment—Part 2-44: Particular requirements for the basic safety and essential performance of X-ray equipment for computed tomography, Third edition (International Electrotechnical Commission, Geneva, Switzerland, 2009).

8 Kalender, W. A. *Computed Tomography. Fundamentals, System Technology, Image Quality, Applications,* 2nd revised edition (Publicis Corporate Publishing, Erlangen, Germany, 2005).
9 Silverman, P. M. (editor). *Multislice Computed Tomography. A Practical Approach to Clinical Protocols* (Lippincott Williams & Wilkins, Philadelphia, PA, 2002).
10 Stern, S. H. Nationwide Evaluation of X-Ray Trends (NEXT) Tabulation and Graphical Summary of 2000 Survey of Computed Tomography, CRCPD Publication E-07-2, (Conference of Radiation Control Program Directors, Inc., Frankfort, KY, 2007).
11 Spelic, D. C. "Nationwide Expansion of X-Ray Trends." (Preliminary results of the 2005–06 NEXT survey of CT), in the Proceedings of 39th Annual National Conference on Radiation Control, CRCPD Publication E-07-4, pp. 98–100 (Conference of Radiation Control Program Directors, Inc., Frankfort, KY, 2007).
12 Benchmark Report. CT 2006, (IMV Medical Information Division, Des Plaines, IL, 2006).
13 Brenner, D. J. (2005). "Is it time to retire the CTDI for quality assurance and dose optimization?" *Med Phys* 32(10):3225–3226.
14 Dixon, R. L. (2006). "Restructuring CT dosimetry—A realistic strategy for the future. Requiem for the pencil chamber." *Med Phys* 33(10):3973–3976.
15 Boone, J. M.. (2007). "The trouble with $CTDI_{100}$." *Med Phys* 34(4):1364–1371.
16 Perisinakis, K., J. Damilakis, A. Tzedakis, A. Papadakis, N. Theocharopoulos, and N. Gourtsoyiannis. (2007). "Determination of the weighted CT dose index in modern multi-detector CT scanners." *Phys Med Biol* 52(21):6485–6495.
17 Huda, W., and K. M. Ogden. (2008). "Comparison of head and body organ doses in CT." *Phys Med* Biol 53(2):N9–N14.
18 Dixon, R. L. (2003). "A new look at CT dose measurement: Beyond CTDI." *Med Phys* 30(6): 1272–1280.
19 Morgan, H.T. (2004). "Beyond CTDI dose measurements for modern CT scanners." Abstract TH-C-317-06. *Med Phys* 31(6):1842.
20 Nakonechny, K.D., B. G. Fallone, and S. Rathee. (2005). "Novel methods of measuring single scan dose profiles and cumulative dose in CT." *Med Phys* 32(1):98–109.
21 Mori, S., M. Endo, K. Nishizawa, T. Tsunoo, T. Aoyama, H. Fujiwara, and K. Murase. (2005). "Enlarged longitudinal dose profiles in cone-beam CT and the need for modified dosimetry." *Med Phys* 32(4):1061–1069.
22 Anderson, J., D. Chason, G. Arbique, and T. Lane. (2005). "New approaches to practical CT dosimetry." Abstract SU-FF-I-14. *Med Phys* 32(6):1907.
23 Dixon, R.L., M.T. Munley, and E. Bayram. (2005). "An improved analytical model for CT dose simulation with a new look at the theory of CT dose." *Med Phys* 32(12):3712–3728.
24 Mori, S., K. Nishizawa, M. Ohno, and M. Endo. (2006). "Conversion factor for CT dosimetry to assess patient dose using a 256-slice CT scanner." *Br J Radiol* 79(947):888–892.
25 Fahrig, R., R. L. Dixon, T. Payne, R. L. Morin, A. Ganguly, and N. Strobel. (2006). "Dose and image quality for a cone-beam C-arm CT system." *Med Phys* 33(12):4541–4550.
26 Amer, A., T. Marchant, J. Sykes, J. Czajka, and C. Moore. (2007). "Imaging doses from the Elekta Synergy X-ray cone beam CT system." *Br J Radiol* 80(954):476–482.
27 Dixon, R. L., and A. C. Ballard. (2007). "Experimental validation of a versatile system of CT dosimetry using a conventional ion chamber: Beyond $CTDI_{100}$." *Med Phys* 34(8):3399–3413.
28 Zhang, D., A. S. Savandi, J. J. Demarco, C. H. Cagnon, E. Angel, A. L. Turner, D. D. Cody et al. (2009). "Variability of surface and center position radiation dose in MDCT: Monte Carlo simulations using CTDI and anthropomorphic phantoms." *Med Phys* 36(3):1025–1038.

29 Gagne, R. M. (1989). "Geometrical aspects of computed tomography: Sensitivity profile and exposure profile." *Med Phys* 16(1):29–37.
30 McCollough, C.H., and F. E. Zink. (1999). "Performance evaluation of a multi-slice CT system." *Med Phys* 26(11):2223–2230.
31 Toth, T. L., N. B. Bromberg, T. S. Pan, J. Rabe, S. J. Woloschek, J. Li, and G. E. Seidenschnuk. (2000). "A dose reduction x-ray beam positioning system for high-speed multislice CT scanners." *Med Phys* 27(12):2659–2668.
32 Paulson, E. W., D. H. Sheafor, D. S. Enterline, H. P. McAdams, and T. T. Yoshizumi. (2001). "CT fluoroscopy-guided interventional procedures: Techniques and radiation dose to radiologists." *Radiology* 220(1):161–167.
33 Hohl, C., C. Suess, J. E. Wildberger, D. Honnef, M. Das, G. Mühlenbruch, A. Schaller, R. W. Günther, and A. H. Mahnken. (2008). "Dose reduction during CT fluoroscopy: Phantom study of angular beam modulation." *Radiology* 246(2):519–525.
34 Kitagawa, K., A. C. Lardo, J. A. C. Lima, and R. T. George. (2009). "Prospective ECG-gated 320 row detector computed tomography: Implications for CT angiography and perfusion imaging," *Int J Cardiovasc Imaging* DOI 10.1007/s10554-009-9433-6, published online 18 February 2009.
35 Shrimpton, P.C. Assessment of Patient Dose in CT. NRPB-PE/1/2004. (National Radiological Protection Board, Chilton, Didcot, Oxon, UK, March 2004).
36 Turner, A., et al. "Comparison of Organ Dose among 64 Detector MDCT Scanners from Different Manufacturers: A Monte Carlo Simulation Study." Paper SSJ23, presented at the 94th Scientific Assembly and Annual Meeting of the Radiological Society of North America, Chicago, November 30–December 5, 2008.
37 Bakalyar, D.M. (2006). "A critical look at the numerical coefficients in $CTDI_{vol}$." *Med Phys* 33(6):2003.
38 Feng, W., C. Culver Schultz, H. Chen, A. Chu, A. Hu, and D. Bakalyar. "Experimental Confirmation of Near Parabolic Shape of Radial Dose Profile in Cylindrical Phantom for Dual Source CT." Poster presentation at the 49th Annual Meeting of the American Association of Physicists in Medicine, Minneapolis, MN, July 22–26, 2007.
39 Nagel, H.D. (editor). *Radiation Exposure in Computed Tomography,* 4th revised and updated edition (CTB Publications, Hamburg, Germany, 2002).
40 Toth, T., Z. Ge, and M. Daly. (2007). "The influence of patient centering on CT dose and image noise." M*ed Phys* 33(7):3093–3101.
41 Zhou, H., and J. M. Boone. (2008). "Monte Carlo evaluation of $CTDI_{\infty}$ in infinitely long cylinders of water, polyethylene and PMMA with diameters from 10 mm to 500 mm." *Med Phys* 35(6): 2424–2431.
42 Ma, C.-M., and A. E. Nahum. (1995). "Calculations of ion chamber displacement effect corrections for medium-energy x-ray dosimetry." *Phys Med Biol* 40:45–62.
43 Seuntjens, J., and F. Verhaegen. (1996). "Dependence of overall correction factor of a cylindrical ionization chamber on field size and depth in medium-energy x-ray beams." *Med Phys* 23: 1789–1796.
44 Mayajima, S. "The Variation of Mean Mass Energy Absorption Coefficient Ratios in Water Phantoms during X-Ray CT Scanning." Proceedings of the 10th EGS4 Users' Meeting in Japan, KEK Proceedings, pp.74–83, 2002-18.
45 van der Molen, A. J., and J. Geleijns. (2007). "Overranging in multisection CT: Quantification and relative contribution to dose—comparison of four 16-section CT scanners." *Radiology* 242(1): 208–216.